Colloids and Surfaces A 583 (2019) 123915

Contents lists available at ScienceDirect

Colloids and Surfaces A

journal homepage: www.elsevier.com/locate/colsurfa

Green synthesis of zirconia nanoparticles based on *Euclea natalensis* plant extract: Optimization of reaction conditions and evaluation of adsorptive properties

Anderson Felipe Viana da Silva[a], Ana Paula Fagundes[a], Domingos Lusitâneo Pier Macuvele[a,b], Elita Fontanele Urano de Carvalho[c], Michelangelo Durazzo[c], Natan Padoin[a], Cíntia Soares[a,*], Humberto Gracher Riella[a]

[a] Laboratory of Materials and Scientific Computing (LabMAC), Department of Chemical and Food Engineering, Federal University of Santa Catarina, Florianópolis, Brazil
[b] Department of Natural Sciences and Mathematics, University of Rovuma-Extension of Niassa, Lichinga, Mozambique
[c] Nuclear and Energy Research Institute - IPEN/CNEN-SP, São Paulo, Brazil

GRAPHICAL ABSTRACT

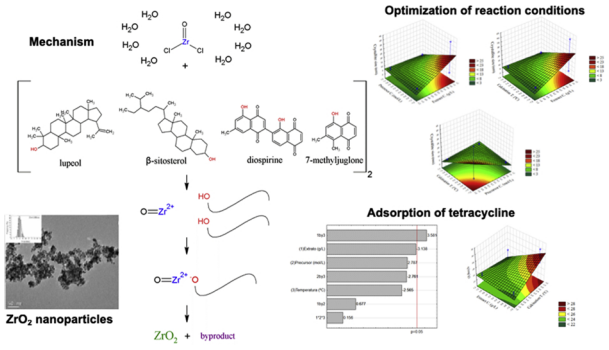

ARTICLE INFO

Keywords:
Zirconia
Nanoparticles
Green synthesis
Euclea natalensis
Adsorption
Tetracycline

ABSTRACT

The development of nanomaterials has attracted increasing attention recently. The study of new technologies to obtain these materials becomes extremely important since the majority of the nanomaterials synthesized require reagents and solvents. These reagents and solvents are sometimes toxic and may generate harmful residues to the environment and the health of living beings. Therefore, green synthesis is a potential alternative to obtain nanoparticles, sustainably, using ecological sources. This study developed a method of synthesizing the green of zirconia (ZrO_2) nanoparticles using *Euclea natalensis* (Natal gwarri or Natal ebony tree with African origin) plant extract. Moreover, the adsorptive properties against tetracycline were evaluated. A factorial design was applied in the synthesis process, and an optimization of the reaction parameters (plant extract concentration, precursor concentration, and calcination temperature) was also described for the first time in literature. The nanoparticles were characterized using the XRD, FTIR and TEM techniques, and then subjected to batch adsorption tests. The samples presented the zirconia monoclinic and tetragonal phases, according to the XRD analysis, yielding materials with minimum crystallite sizes equal to 5.25 nm. The FTIR spectra confirmed the results obtained by the XRD, presenting band characteristic of the zirconia monoclinic and tetragonal phases. The particles had a rounded morphology with a very low average diameter ranging from 5.90 to 8.54 nm. Moreover, the nanoparticles were applied to the adsorption of tetracycline. The samples were synthesized with vegetal extract and

* Corresponding author.
E-mail address: cintia.soares@ufsc.br (C. Soares).

https://doi.org/10.1016/j.colsurfa.2019.123915
Received 29 June 2019; Received in revised form 31 August 2019; Accepted 1 September 2019
Available online 05 September 2019

precursor concentration equal to 50 g L^{-1} and 0.03 mol L^{-1}, respectively, and calcination temperature of 550 °C, presented in the best performance (loading of 30.45 mg g^{-1}). The adsorption capacity of the zirconia synthesized in this study was significantly higher than other common materials applied to tetracycline removal. The green synthesis procedure, as well as the application of the zirconia nanoparticles to the adsorption of an emerging pollutant, were promising.

1. Introduction

Emerging contaminants are compounds that are increasingly found in the environment. Among this class of contaminants, drugs are the ones most studied in the world, because they are constantly released into the environment in large quantities [1–3]. Advances in nano-scale technology have led to the use of nanoparticles in various science branches. Nanotechnology and nanoscience aim to develop nanometer-scale materials (1–100 nm). The great interest in these new materials has to due to their reduced size and new or improved properties when compared to larger particles [4–6].

Zirconium oxide (ZrO_2), also known as zirconia, is a versatile material which has been widely used in applications such as reinforcement of structures, antimicrobial agent, adsorption, and photodegradation [7–11]. It has enhanced thermal, mechanical, catalytic, corrosion, and tribological properties [12].

Methods for the synthesis of zirconia nanoparticles have been investigated in some recent studies [13–15]. However, the conventional methods used require sometimes toxic solvents generating harmful residues to health and the environment. Thus, the green synthesis in the production of nanoparticles is promising [16–19].

Green synthesis is a method that uses non-toxic, biodegradable and low-cost chemicals for the synthesis of nanomaterials [20–23]. Among the biological resources that have potential use in nanoparticles synthesis plant extracts, algae, fungi, and bacteria may be highlighted. Plant extracts are very promising due to their complex chemical composition and the facilities to their extraction. They act in the synthesis as a reducer and as a capping agent preventing the agglomeration of nanoparticles during the crystal growth step [24]. Although there are some studies using green synthesis for the preparation of zirconia nanoparticles [20,25–27], many other contributions are still needed since the great genetic variability of plant species can lead to chemical composition variation depending on the plant studied. This factor can interfere directly in the properties of the material obtained. Because of that, the use of different species must still be evaluated.

Natal gwarri or Natal ebony (*Euclea natalensis*) is a tree of the *Ebenaceae* family with African origin. Species of this genus are rich in chemical compounds classified as naphthoquinones and terpenes. Several applications of these compounds have been reported. Some of their uses are in/as: biomedicine; antioxidant, antibacterial and antifungal activity phytochemistry and pharmacological properties; and acid-base indicator [28–31]. Naphthoquinones have functional groups that may favor a reduction of the metal during synthesis, while the terpenoids can serve as a capping agent due to their low electronic density. Thus, it may facilitate the formation of particles with smaller size and with inhibitory effect by the formation of agglomerates [29].

The proposal of a nanomaterial synthesized from a less environmentally aggressive route (green synthesis) is of paramount importance. Also, the use of the *Euclea natalensis* extract as a reducer in the synthesis of metal oxide nanoparticles is still not reported in the literature. Moreover, the studies found about other species of plants only describe the synthesis and do not mention the optimization of the reaction parameters. Furthermore, the application of zirconia oxide nanoparticles as an adsorbent is not a novelty but it is not reported anywhere for emerging contaminants (tetracycline). Therefore, the present study aims to develop a method to obtain zirconia (ZrO_2) nanoparticles from *Euclea natalensis* plant extract (used as a reducer in the synthesis of a metal oxide nanostructured material for the first time). Moreover, it will be evaluated the effect of the reaction conditions (extract concentration, precursor concentration, and calcination temperature) on the characteristics of the particles obtained as well as their performance as an adsorbent for the treatment of an emerging contaminant (tetracycline).

2. Materials and methods

2.1. Materials

The roots of *Euclea natalensis* were collected in Maputo (Mozambique). Their biological identity was confirmed by the biologist Suzana Macuvele (Museu de Historia Natural-UEM). The analytical grade zirconyl chloride octahydrate ($ZrOCl_2{\cdot}8H_2O$) used was purchased by Neon (Brazil).

2.2. Euclea natalensis extract preparation

Euclea natalensis roots were washed three times with tap water followed by distilled water. After, they were dried in an oven at 60 °C for 24 h and ground in a knife mill (SPLabor MA-340). The powder was mixed with 500 mL of distilled water (with concentration determined according to a factorial design), heated in a water bath at 80 °C for one hour, and stirred in a magnetic stirrer for 20 min. The solution was then filtered and reserved for use.

2.3. Factorial design

The synthesis conditions were determined from a 2^3 factorial design with three central points. The factors and levels varied are shown in Table 1.

The percentage of the tetragonal phase of the samples, the average crystallite size and the amount of tetracycline adsorbed by the synthesized material were used as the factorial design response.

Table 1
Factors and levels of the factorial design applied to the synthesis of zirconia nanoparticles using Euclea natalensis extracts.

Factors	Levels		
	−1	0	+1
01 Extract concentration (g·L^{-1})	50	75	100
02 Precursor concentration (mol·L^{-1})	0.01	0.02	0.03
03 Calcination temperature (°C)	550	600	650

Sample	Extract C. (g L^{-1})	Precursor C. (mol L^{-1})	Calcination T. (°C)
01	100	0.03	650
02	100	0.03	550
03	100	0.01	650
04	100	0.01	550
05	50	0.03	650
06	50	0.03	550
07	50	0.01	650
08	50	0.01	550
09	75	0.02	600
10	75	0.02	600
11	75	0.02	600

2.4. Green synthesis of zirconia nanoparticles

Initially, 300 mL of zirconyl chloride solution was prepared and added to a jacketed reactor with stirring at 900 rpm. 300 mL of *Euclea natalensis* extract was added dropwise, with the aid of a peristaltic pump in an average feed of 3.5 mL min^{-1}. This mixture was stirred for 3 h. The dark color solution was then reserved and oven-dried at 105 °C for 24 h. The precipitate, also dark-colored, was triturated in a mortar and it was calcined in a muffle, according to the temperature determined in the factorial design, for 3 h. The white powder obtained was stored in Eppendorf flasks for further characterization.

2.5. Zirconia nanoparticles characterization

The white powder obtained was characterized by X-ray diffraction (XRD) on Shimadzu diffractometer (LabX XRD-6100) with 2θ ranging from 10 to 50° in steps of 0.02° and acquisition time of 1 s per step, the temperature of 25 °C and using the Kα line of copper (0.1542 nm). The XRDs were analyzed using X'pert Highscore Plus software for the identification of the crystalline phase. The average crystallite sizes were obtained using the Scherrer equation [Eq. (1)] estimated using the software Origin 8.0 [32].

$$D_{XRD} = \frac{K\lambda}{\beta \cos\theta} \quad (1)$$

where K is the constant that depends on the shape of the particles (equal to 0.9 for spherical particles), λ is the X-ray wavelength, θ is the angle of Bragg diffraction and β is the difference between the full width at half maximum and the instrumental broadening.

The identification of functional groups was performed by Fourier Transform Infrared Spectroscopy (FTIR) on Shimadzu FTIR Spectrophotometer (IR Prestige-21). Also, the material was characterized by Transmission Electron Microscopy (TEM) using a JEM-1011 TEM microscope (TEM 100 kV). Finally, the particle diameter (D_{TEM}) was obtained by measuring 100 particles using the software ImageJ®.

2.6. Batch adsorption

In each experiment, 20 mL of tetracycline solution (20 mg L^{-1}) and 10 mg of adsorbent, under different conditions according to the factorial design, were used. The mixture was stirred for 24 h at neutral pH and at the temperature of 25 °C. The supernatants were centrifuged and filtered on 20 μm filters (CHROMAFIL®). and The concentration of each solution was determined in a UV–vis spectrophotometer at the wavelength of 357 nm using the Lambert-Beer law [33]. The tetracycline loading was determined according to Eq. (2).

$$q_e = \frac{(C_o - C_e)V}{m} \quad (2)$$

where q_e is the load of tetracycline adsorbed, C_o is the initial concentration, C_e is the final concentration of tetracycline at the solution, V is the volume of aqueous solution used in liters and m the mass of adsorbent used.

3. Results and discussion

3.1. XRD

Fig. 1 shows the diffractograms obtained for the synthesized samples. There is a certain similarity between all the samples, presenting the same peak characteristic of the monoclinic and tetragonal phases of zirconia.

The percentage composition of the phases contained in each sample is showed in Table 2. The diffractograms, except for sample 04, present intense peak characteristic of the tetragonal phase (ICSD 072951). Samples 05 and 06 presented the highest percentage of tetragonal zirconia (82% and 79%, respectively), while sample 04 yielded the highest percentage (56%) of monoclinic zirconia (ICSD 060901). Most of the samples present mainly the tetragonal phase.

Table 2
Phases contained in the synthesized zirconia nanoparticles, crystallite size (D_{XRD}) calculated from the Sherrer equation and mean particle diameter (D_{TEM}) obtained from TEM images.

Sample	Crystalline phase		D_{XRD} (nm)	D_{TEM} (nm)
	Monoclinic (%)	Tetragonal (%)		
01	26	74	7.20	8.53
02	31	69	5.72	6.19
03	40	60	5.82	6.81
04	56	44	41.71	–
05	18	82	8.19	8.30
06	21	79	6.03	5.90
07	34	66	5.94	8.49
08	39	61	5.25	7.47
09	31	69	6.00	8.29
10	28	72	6.27	8.54
11	30	70	5.88	8.10

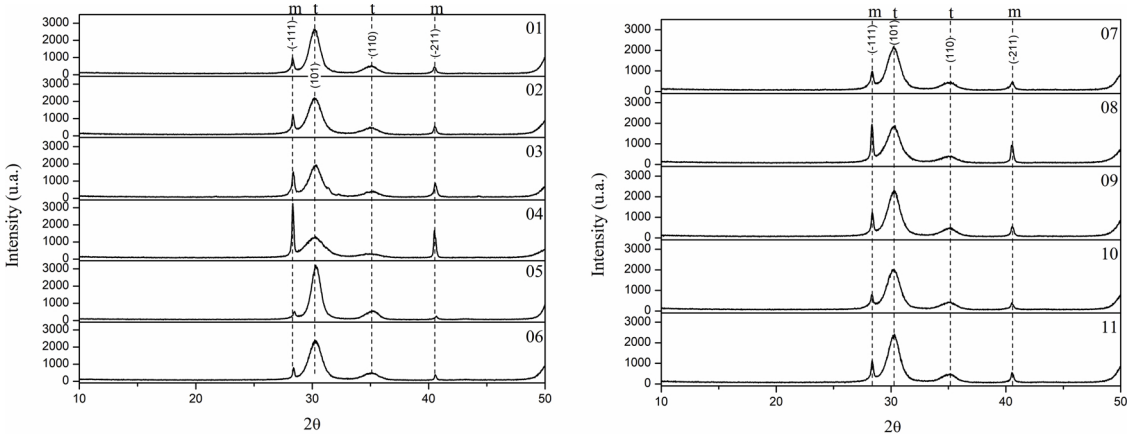

Fig. 1. Diffractograms of the synthesized zirconium oxide nanoparticles, where m is the characteristic peak of zirconia monoclinic phase and t is the characteristic peak of zirconia tetragonal phase.

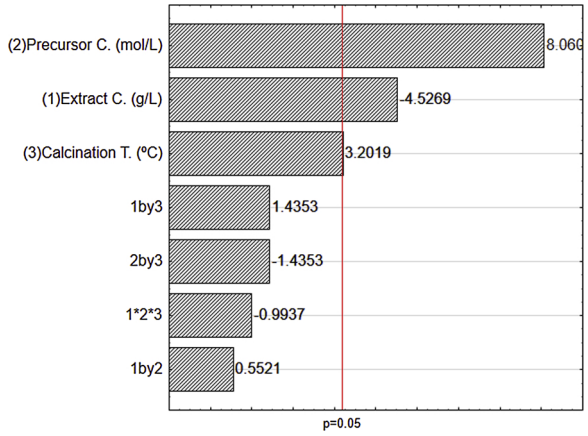

Fig. 2. Pareto chart for the tetragonal phase percentage of the synthesized nanoparticles.

Fig. 2 shows the Pareto chart concerning the percentage of the tetragonal phase of the nanoparticles obtained.

The increase of the precursor concentration in the synthesis favored significantly to obtain nanoparticles with a greater percentage of the tetragonal phase. The same behavior was observed regarding the calcination temperature, where a higher temperature favors the formation of the tetragonal phase. In contrast, the plant extract concentration had a negative effect on the process, i.e., a lower extract concentration favored the tetragonal phase of zirconium oxide nanoparticles. This is a key feature through a green chemistry perspective since the beneficial use of lower extract concentrations will lead to a smaller amount of the material to be used in the synthesis [34].

Even after the sample calcination process, at the studied temperatures, it is normal to obtain samples with a phase mixture [26,35]. Particles with the tetragonal phase have lower surface energy rather than those with the monoclinic phase when the particle size is very small. Asa result, smaller particles are preferably stabilized with the tetragonal structure [36,37].

Table 2 also shows the crystallite size (D_{XRD}) obtained for the zirconia nanoparticles synthesized. Sample 04, with a higher percentage of monoclinic phase, presented the largest crystallite size. The significant factors are highlighted in the Pareto chart presented in Fig. 3(a).

The first-order factors were not significant in the process when evaluating the crystallite size response. However, all second-order interaction factors were significant, indicating that the relationship between the factors directly interferes in the crystallite size of the particles obtained. In order to understand how each of these relations interferes in the crystallite size, the surface response graphs were obtained for each second-order interaction.

Fig. 3(b), shows the interaction between the extract and precursor

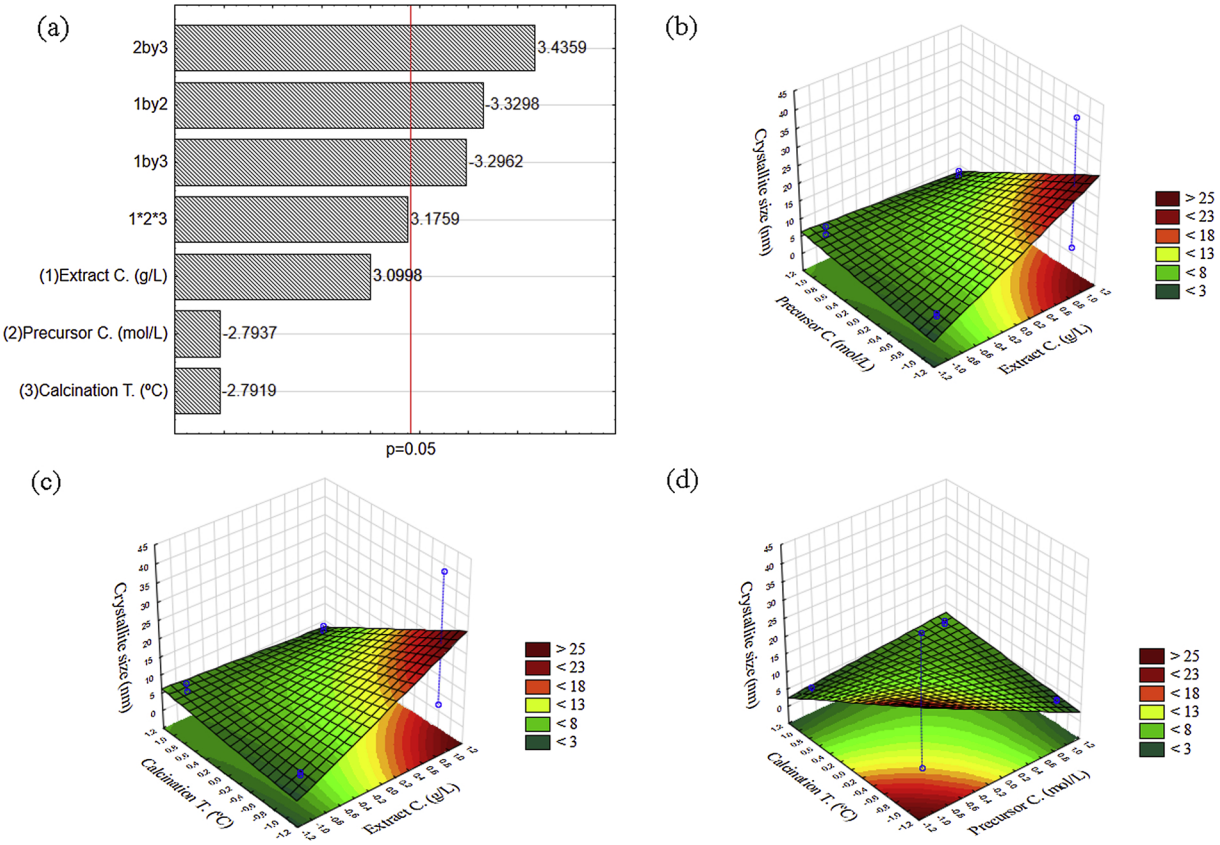

Fig. 3. (a) Pareto chart and response surface for the interaction between (b) extract concentration and precursor concentration, (c) extract concentration and calcination temperature and (d) precursor concentration and calcination temperature with respect to the crystallite size.

concentrations. It is possible to observe that by maintaining the precursor concentration fixed at the lower level and moving from the lower to the higher level of the extract concentration, the results are increasing considerably in the crystallite size obtained. On the other hand, fixing the precursor concentration at the higher level and shifting from the lower to the higher level of extract concentration resulted in the opposite behavior, but with lower intensity. The exchange of the extract and precursor concentrations results in the opposite effect.

The same behavior is observed when the precursor concentration factor is replaced by the calcination temperature [Fig. 3(c)]. The response surfaces are almost identical, this was expected since the effect observed on the Pareto chart has the same signal and almost the same intensity.

Fig. 3(d) shows the interaction of the calcination temperature and the concentration of precursor. In this case, the results of keeping the calcination temperature at the lower level and moving from the lower to the higher level of precursor concentration are smaller crystallite sizes. However, the results of fixing the calcination temperature at the higher level and moving from the lower to the higher level of precursor concentration were an increase in the crystallites size, but with lower intensity, remaining = stable. Similarly, the results of exchanging the calcination temperature and precursor concentration were the opposite effects. The effect of increasing the crystallite size when increasing the calcination temperature in the synthesis of zirconia nanoparticles was already reported in the literature [38–40]. The same behavior was observed herein (i.e., smaller crystallite sizes with lower calcination temperature, maintaining the same precursor and extract concentrations), except for the sample 04.

3.2. FTIR

Fig. 4 illustrates the FTIR spectra of all samples. All the spectra presented the same peaks, varying only the intensity. It has also indicated that all the synthesized samples presented some similarity regarding the chemical bonds and the functional groups.

In the region between 3200 and 3600 cm^{-1}, it is possible to observe a large band with variable intensity between the samples. This was equivalent to the stretching vibrations of the −OH group, probably resulting from the presence of residual water from the synthesis or adsorbed from the atmosphere. At 1600 cm^{-1}, a weak band was assigned to bending vibration of physically adsorbed H_2O [15].

In the region between 980 and 1180 cm^{-1} two intense peaks around 1014 and 1140 cm^{-1} can be highlighted. Peaks between 980 and 1100 cm^{-1} usually indicate the presence of Zr-O binding bands characteristic of the tetragonal phase of zirconia, and the presence of a peak at 1140 cm^{-1} may refer to a small translation of the tetragonal phase [15].

Furthermore, the peaks found around 460 and 620 cm^{-1} have been reported as results from the monoclinic phase of the material, corroborating with the results obtained in the XRD, where a mixture of the monoclinic and tetragonal phases of the material was observed in all the samples synthesized [41].

3.3. TEM

The morphology of zirconium oxide nanoparticles was evaluated by TEM (Fig. 5) and it was observed that the synthesized particles presented a spherical shape. In addition, it is possible to note that the particles tend to form agglomerates, a common feature of nanoparticles. The particle size distribution images can be viewed on supplementary material (Figure S1).

The frequency distributions, obtained to determine the particles size from the transmission microscopy images (D_{TEM}), showed a low dispersion that may indicate a certain homogeneity between the size of the nanoparticles (Table 2). It was not possible to obtain the mean diameter of the particles of sample 04, since, in the images obtained, the nanoparticles were very agglomerated and it was not possible to separate the particle from the agglomerate. Furthermore, the particle size obtained by TEM is in agreement with the crystallite size measured by XRD. This behavior suggests that the measurement is more accurate and the obtained zirconium oxide nanoparticles present particles with homogenous morphology [42]. It was not possible to obtain the behavior from factorial design for this response since there was no response from the sample 04.

Table 3 shows the particle size obtained in previous works using different plant extracts. It is possible to observe that the nanoparticles synthesized in this work have presented a very small size, below 10 nm, which indicates that the use of *Euclea natalensis* extract is promising.

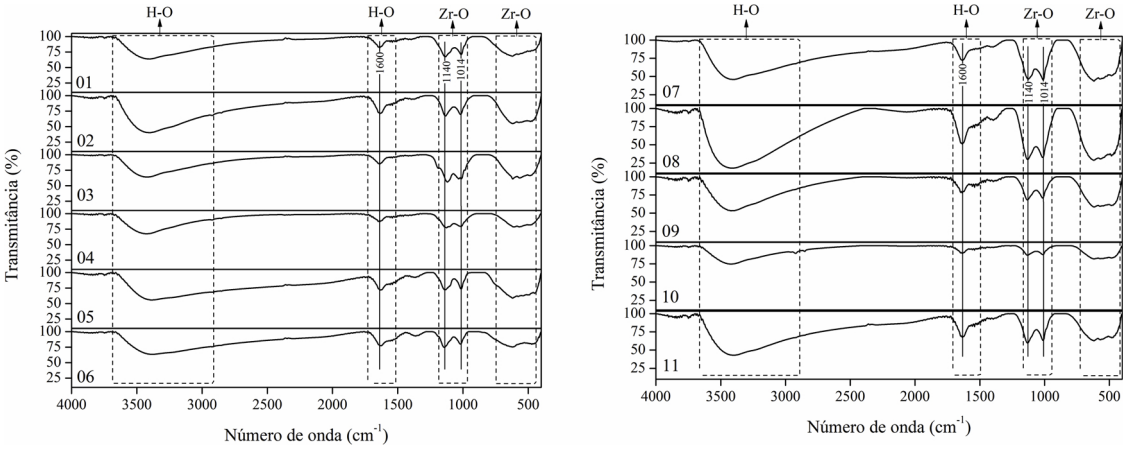

Fig. 4. FTIR spectra of the zirconium oxide nanoparticles synthesized.

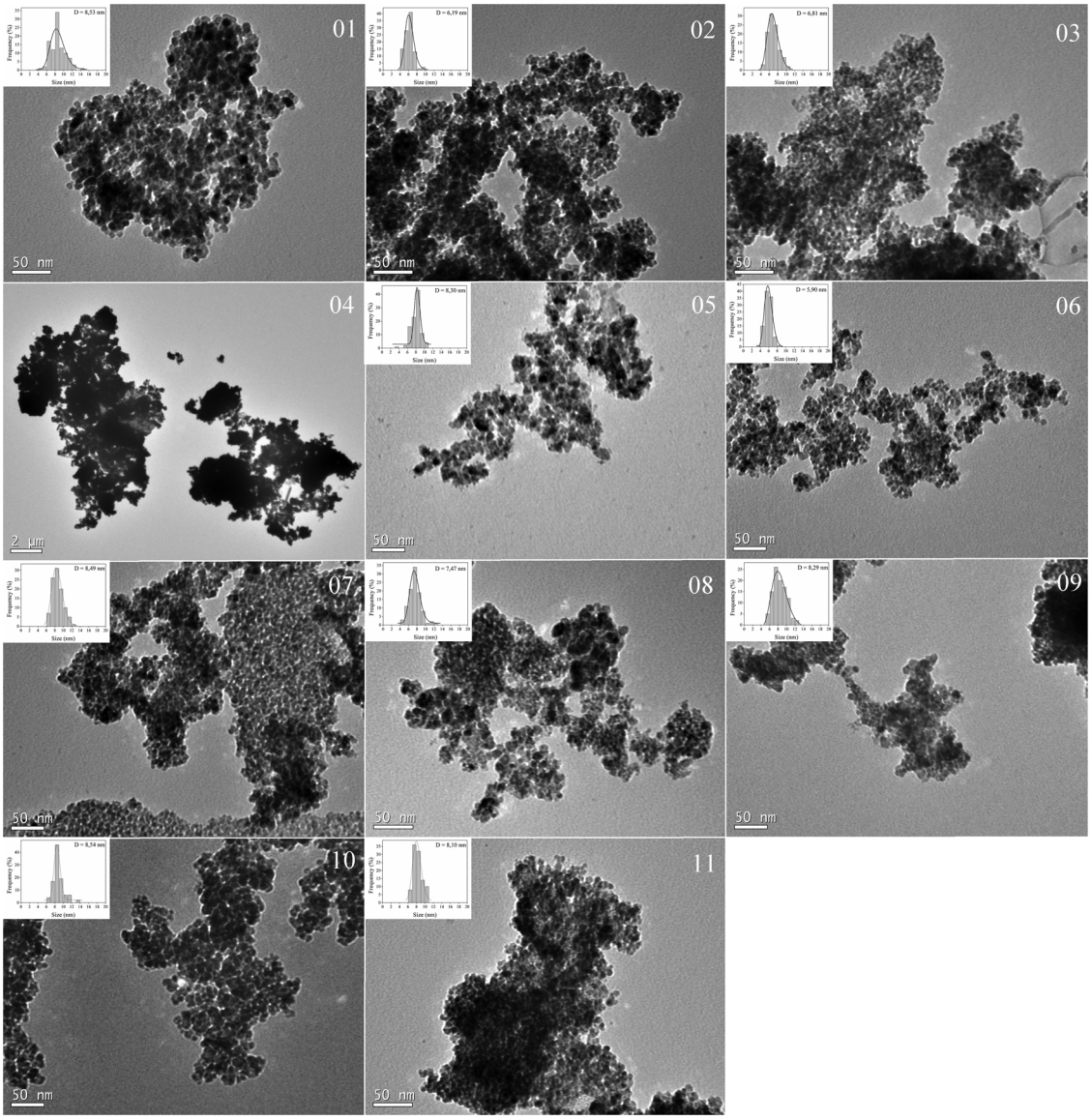

Fig. 5. Transmission Electron Microscopy (TEM) images and frequency distribution of the particle diameter of the zirconium oxide nanoparticles synthesized.

Table 3
Particle size obtained for zirconia nanoparticles synthesized in previous works using different plant extracts.

Plant Extract	Particle Diameter (nm)	Ref.
Euclea natalensis	5.90–8.54	This work
Eucalyptus globulus	9–11	[20]
Rosmarinus officinalis	~ 16	[43]
Lagerstroemia speciosa	~ 56	[44]
Curcuma longa	41–45	[26]

3.4. Synthesis mechanism proposed

The mechanism for the reduction and stabilization of zirconia nanoparticles from biomolecules is still poorly described in the literature. The formation of the nanoparticles consists mainly of three stages: the reduction of ions, the grouping of nanoparticles and the nanoparticles' subsequent growth. The characteristics of each stage depend on the nature of the reducing agent, its concentration, and reaction conditions [16].

A possible mechanism for the synthesis of the zirconia nanoparticles was proposed based on the basic reaction equation of zirconia formation from the reduction zirconyl chloride [45,46] and considering the major biological compounds already reported in the *Euclea natalensis* roots extract [29] as it is shown in Fig. 6.

The four compounds used in this proposal are pentaciclic terpenoids (lupeol, betulin and β-sitosterol) and naphthoquinones (diospirine, shinanolone and 7-methyljuglone) (Table 4 and Figure S2). The −OH groups present in these biomolecules, such as quercetin, may be responsible for the reduction of the nanoparticles [16,47]. It is possible that the tautomeric transformation of the enol compounds into the keto form releases the reactive hydrogen atom, which reduces the ions of the molecule with zirconium. As a result, after the calcination, it has the nanoparticles of zirconia since at the temperatures used the organic matter presented after the reaction is removed [48]. The biomolecule, besides acting as an ion reducer, also assists in the termination process,

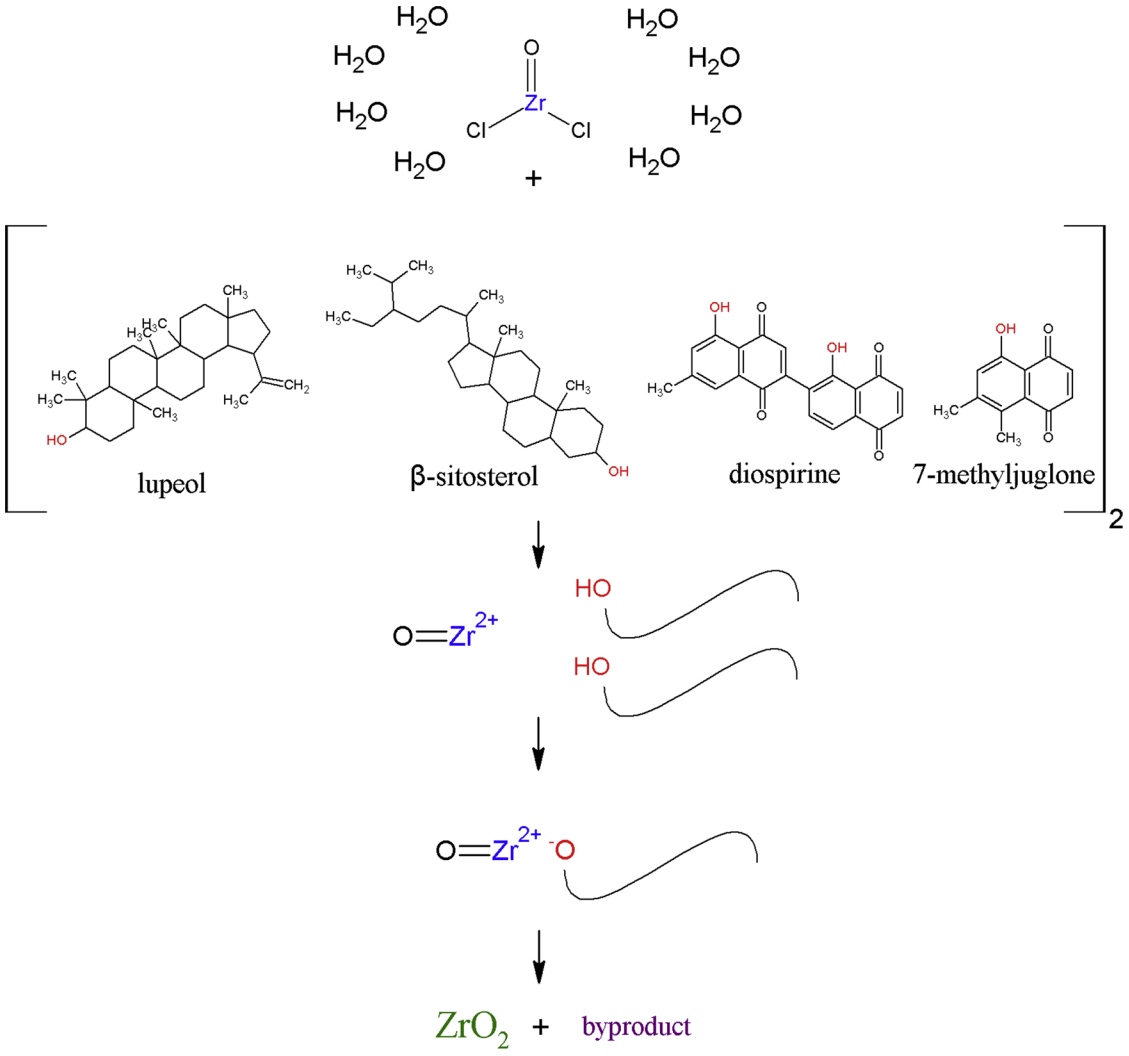

Fig. 6. Proposed mechanism for the synthesis of ZrO_2 nanoparticles via different biological compounds.

Table 4
Terpenoids and naphthoquinones reported in the literature as present in *Euclea natalensis* roots, adapted from [29].

Compouds	Chemical formula	Classification	Ref.
Shinanolone	$C_{11}H_{12}O_3$	naphtoquinone	[50]
Diospyrin	$C_{22}H_{14}O_6$	naphtoquinone	[51]
7-methyljuglone	$C_{11}H_8O_3$	naphtoquinone	[52]
Betulin	$C_{30}H_{50}O_2$	terpenoids	[53]
Lupeol	$C_{30}H_{50}O$	terpenoids	[54]
β-sisterol	$C_{29}H_{50}O$	terpenoids	[54]

once the rest of its chain serves as a stabilizer for the nanoparticle formed, avoiding its agglomeration [49].

3.5. Adsorption

Fig. 7 shows the amount of tetracycline adsorbed in each sample. In addition, a test of comparison of means was executed to determine if there is a significant difference between the samples. Sample 06 presented the best adsorptive capacity, followed by samples 08 and 02. Although sample 06 did not yield the smallest crystallite size (according to the X-ray diffractograms), it presented a larger percentage of tetragonal phase, what may justify its superior adsorption performance [36]. Moreover, the transmission electron microscopy images indicated that sample 06 presented the smaller mean particle diameter (and, consequently, the higher surface-to-volume ratio) when compared to all nanoparticles synthesized.

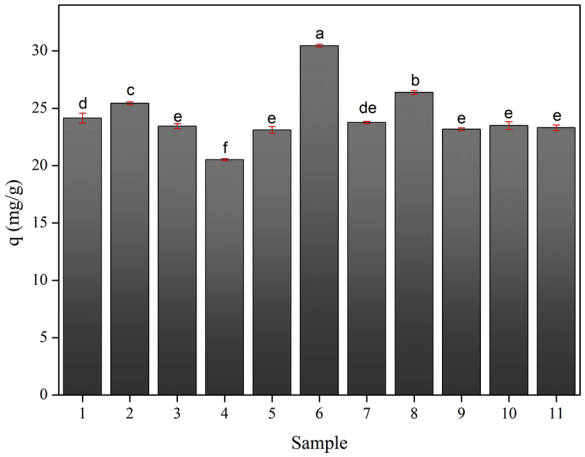

Fig. 7. Results of batch adsorption for the synthesized nanoparticles (Samples identified with the same letter did not present significant difference ($p < 0.05$) in the Tukey test).

Table 5 presents a comparison of the adsorption capacity obtained in the present work with different adsorbents tested against tetracycline. The synthesized nanoparticles have a promising adsorptive

Table 5
Adsorptive capacity of tetracycline for different adsorbents.

Adsorbent	C_o (mg/L)	Adsorbent concentration (g/L)	q_e (mg/g)	Ref.
Zirconia nanoparticles	20	0.5	30.45	This work
Nanocrystalline cellulose	20	1.5	5.66	[55]
Rice straw	32	3.0	14.16	[56]
RCGEM	50	2.0	19.02	[57]

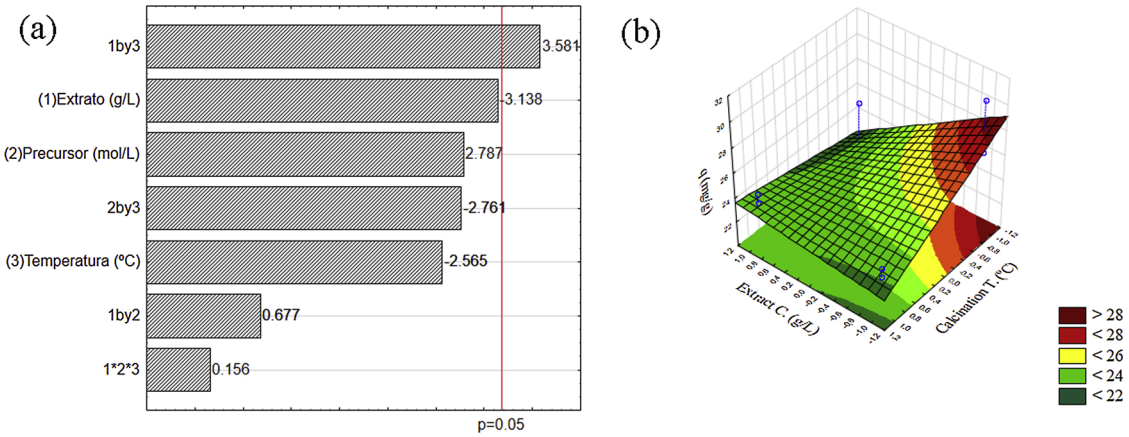

Fig. 8. (a) Pareto chart and (b) response surface for the interaction between the extract concentration and calcination temperature with respect to the tetracycline adsorption.

capacity, being the first work to test this material as a tetracycline adsorbent.

The adsorptive capacity of the material was also characterized as a factorial response. According to Pareto chart [Fig. 8(a)], only the interaction between the extract concentration and the calcination temperature was significant in the process ($p < 0.05$). Thus, the response surface that relates these two factors were generated [Fig. 8(b)].

There is a decrease in the adsorptive capacity of the material When fixing the extract concentration at the lower level and moving from the lower to the higher level of the calcination temperature. The same behavior is observed when the calcination temperature is fixed at the lower level and one moves from the lower to the higher level of the extract concentration factor. In contrast, the effect is the opposite when setting one of the factors at the higher level.

Therefore, the nanoparticles obtained with extract concentration of 50 g L^{-1} and calcination temperature of 550 °C should present the optimal performance, regardless of the precursor concentration. This evidence was confirmed herein since samples 06 and 08 presented the best performance and were prepared using the synthesis conditions previously mentioned.

4. Conclusions

The method proposed for the synthesis of zirconia nanoparticles using *Euclea natalensis* root extract was effective, and materials with monoclinic and tetragonal phases were obtained. The factorial design showed that the first-order factors were significant for the phase composition, where a higher concentration of precursor, lower concentration of vegetal extract and higher calcination temperature favored the formation of the zirconia tetragonal phase.

The nanoparticles presented a crystallite size ranging from 5.25 to 41.71 nm. For this response variable, the second-order interaction among the factors was significant in the process. In the infrared spectra analysis (FTIR), the characteristic bands obtained corroborated the XRD results, presenting Zr-O binding bands characteristic of the monoclinic and tetragonal phases. Moreover, TEM images indicated that spherical nanoparticles with very small average diameters (5.90 nm – 8.54 nm) were produced.

Furthermore, sample 06 (with a larger percentage of tetragonal phase) presented the best adsorptive capacity for tetracycline (30.45 mg g^{-1}), indicating that the interaction between the extract concentration and the calcination temperature is significant for the adsorption process.

Declaration of Competing Interest

The authors declare that they have no known competing financial interests or personal relationships that could have appeared to influence the work reported in this paper.

Acknowledgements

The authors acknowledge the National Council for Scientific and Technological Development (CNPq), the Coordination for the Improvement of Higher Education Personnel (CAPES), the Central Laboratory of Electron Microscopy (LCME) and the Federal University of Santa Catarina (UFSC).

Appendix A. Supplementary data

Supplementary material related to this article can be found, in the online version, at doi:https://doi.org/10.1016/j.colsurfa.2019.123915.

References

[1] M. Gavrilescu, K. Demnerová, J. Aamand, S. Agathos, F. Fava, Emerging pollutants in the environment: present and future challenges in biomonitoring, ecological risks and bioremediation, N. Biotechnol. 32 (2015) 147–156, https://doi.org/10.1016/J.NBT.2014.01.001.
[2] C.C. Montagner, C. Vidal, R.D. Acayaba, Contaminantes emergentes em matrizes aquáticas do Brasil: Cenário atual e aspectos analíticos, ecotoxicológicos e regulatórios, Quim. Nova 40 (2017) 1094–1110, https://doi.org/10.21577/0100-4042.20170091.
[3] B. Petrie, R. Barden, B. Kasprzyk-Hordern, A review on emerging contaminants in

wastewaters and the environment: current knowledge, understudied areas and recommendations for future monitoring, Water Res. 72 (2015) 3–27, https://doi.org/10.1016/J.WATRES.2014.08.053.
[4] M.C. Roco, N.S. Foundation, U.S.N. Science, N. Science, International strategy for nanotechnology research and development, J. Nanopart. Res. 3 (2001) 353–360.
[5] T.M. Sakr, M.F. Nawar, T.W. Fasih, S. El-Bayoumy, H.A. Abd El-Rehim, Nanotechnology contributions towards the development of high performance radioisotope generators: the future promise to meet the continuing clinical demand, Appl. Radiat. Isot. 129 (2017) 67–75, https://doi.org/10.1016/j.apradiso.2017.08.012.
[6] S.S. Su, I. Chang, Review of production routes of nanomaterials, Commer. Nanotechnologies – A Case Study Approach, Springer International Publishing, 2017, pp. 15–29, https://doi.org/10.1007/978-3-319-56979-6.
[7] J. Bani, A. Pugazhendhi, R. Venis, Synthesis and characterization of ZrO 2 nanoparticles-antimicrobial activity and their prospective role in dental care, Microb. Pathog. 110 (2017) 245–251, https://doi.org/10.1016/j.micpath.2017.06.039.
[8] R. Chakravarty, R. Shukla, R. Ram, A.K. Tyagi, A. Dash, M. Venkatesh, Practicality of Tetragonal Nano-Zirconia as a prospective sorbent in the preparation of 99Mo/99mTc generator for biomedical applications, Chromatographia 72 (2010) 875–884, https://doi.org/10.1365/s10337-010-1754-z.
[9] D. Manoharan, A. Loganathan, V. Kurapati, V.J. Nesamony, Unique sharp photoluminescence of size-controlled sonochemically synthesized zirconia nanoparticles, Ultrason. Sonochem. 23 (2015) 174–184, https://doi.org/10.1016/j.ultsonch.2014.10.004.
[10] F. Tana, M. Messori, D. Contini, A. Cigada, T. Valente, F. Variola, L. De Nardo, F. Bondioli, Synthesis and characterization of scratch-resistant hybrid coatings based on non-hydrolytic sol-gel ZrO 2 nanoparticles, Prog. Org. Coat. 103 (2017) 60–68, https://doi.org/10.1016/j.porgcoat.2016.11.022.
[11] K. Vignesh, A. Suganthi, B. Min, M. Kang, Fabrication of meso-porous BiOI sensitized zirconia nanoparticles with enhanced photocatalytic activity under simulated solar light irradiation, Appl. Surf. Sci. 324 (2015) 652–661, https://doi.org/10.1016/j.apsusc.2014.11.004.
[12] S. Sagadevan, J. Podder, I. Das, Hydrothermal synthesis of zirconium oxide nanoparticles and its characterization, J. Mater. Sci. Mater. Electron. 27 (2016) 5622–5627, https://doi.org/10.1007/s10854-016-4469-6.
[13] T. Ahmad, M. Shahazad, R. Phul, Hydrothermal synthesis, characterization and dielectric properties of zirconia nanoparticles, Mater. Sci. Eng. Int. 1 (2017) 4–8, https://doi.org/10.15406/mseij.2017.01.00017.
[14] S. Zinatloo-ajabshir, M. Salavati-niasari, Facile route to synthesize zirconium dioxide (ZrO 2) nanostructures: structural, optical and photocatalytic studies, J. Mol. Liq. 216 (2016) 545–551, https://doi.org/10.1016/j.molliq.2016.01.062.
[15] R. Dwivedi, A. Maurya, A. Verma, R. Prasad, K.S. Bartwal, Microwave assisted sol – gel synthesis of tetragonal zirconia nanoparticles, J. Alloys. Compd. 509 (2011) 6848–6851, https://doi.org/10.1016/j.jallcom.2011.03.138.
[16] V.V. Makarov, A.J. Love, O.V. Sinitsyna, S.S. Makarova, I.V. Yaminsky, M.E. Taliansky, N.O. Kalinina, "Green" nanotechnologies: synthesis of metal nanoparticles using plants, Acta Nat. 6 (2014) 35–44, https://doi.org/10.1039/c1gc15386b.
[17] Y.X. Zhang, J. Zheng, G. Gao, Y.F. Kong, X. Zhi, K. Wang, X.Q. Zhang, D.X. Cui, Biosynthesis of gold nanoparticles using chloroplasts, Int. J. Nanomed. 6 (2011) 2899–2906, https://doi.org/10.2147/IJN.S24785.
[18] A. Sebastian, A. Nangia, M.N.V. Prasad, A green synthetic route to phenolics fabricated magnetite nanoparticles from coconut husk extract: Implications to treat metal contaminated water and heavy metal stress in Oryza sativa L, J. Clean. Prod. 174 (2018) 355–366, https://doi.org/10.1016/J.JCLEPRO.2017.10.343.
[19] D. Qin, G. Yang, Y. Wang, Y. Zhou, L. Zhang, Green synthesis of biocompatible trypsin-conjugated Ag nanocomposite with antibacterial activity, Appl. Surf. Sci. 469 (2019) 528–536, https://doi.org/10.1016/J.APSUSC.2018.11.057.
[20] S. Balaji, B.K. Mandal, S. Ranjan, N. Dasgupta, R. Chidambaram, Nano-zirconia – evaluation of its antioxidant and anticancer activity, J. Photochem. Photobiol. B Biol. 170 (2017) 125–133, https://doi.org/10.1016/j.jphotobiol.2017.04.004.
[21] M. Kumaresan, K.V. Anand, K. Govindaraju, S. Tamilselvan, V.G. Kumar, Seaweed Sargassum wightii mediated preparation of zirconia (ZrO 2) nanoparticles and their antibacterial activity against gram positive and gram negative bacteria, Microb. Pathog. 124 (2018) 311–315, https://doi.org/10.1016/j.micpath.2018.08.060.
[22] T. Wang, K. Li, S. An, C. Song, X. Guo, Facile and green synthesis of TiN/C as electrode materials for supercapacitors, Appl. Surf. Sci. 470 (2019) 241–249, https://doi.org/10.1016/J.APSUSC.2018.11.088.
[23] N.F. Attia, J. Park, H. Oh, Facile tool for green synthesis of graphene sheets and their smart free-standing UV protective film, Appl. Surf. Sci. 458 (2018) 425–430, https://doi.org/10.1016/J.APSUSC.2018.07.066.
[24] D. Nath, P. Banerjee, Green nanotechnology - a new hope for medical biology, Environ. Toxicol. Pharmacol. 36 (2013) 997–1014, https://doi.org/10.1016/j.etap.2013.09.002.
[25] A. Nikam, T. Pagar, S. Ghotekar, K. Pagar, S. Pansambal, A review on plant extract mediated green synthesis of zirconia nanoparticles and their miscellaneous applications, J. Chem. Rev. 1 (2019) 154–163, https://doi.org/10.33945/SAMI/JCR.2019.3.
[26] M. Sathishkumar, K. Sneha, Y.-S. Yun, Green fabrication of zirconia nano-chains using novel Curcuma longa tuber extract, Mater. Lett. 98 (2013) 242–245, https://doi.org/10.1016/J.MATLET.2013.02.036.
[27] V. Bansal, D. Rautaray, A. Ahmad, M. Sastry, Biosynthesis of zirconia nanoparticles using the fungus Fusarium oxysporum, J. Mater. Chem. 14 (2004) 3303–3305.
[28] N. Lall, V. Kumar, D. Meyer, N. Gasa, C. Hamilton, M. Matsabisa, C. Oosthuizen, In vitro and In vivo antimycobacterial, hepatoprotective and immunomodulatory activity of Euclea natalensis and its mode of action, J. Ethnopharmacol. 194 (2016) 740–748, https://doi.org/10.1016/J.JEP.2016.10.060.
[29] A. Maroyi, Review of ethnomedicinal uses, phytochemistry and pharmacological properties of Euclea natalensis A.DC, Molecules 22 (2017) 2128, https://doi.org/10.3390/molecules22122128.
[30] S.H. Chauke, N. Lall, Q. Kritzinger, Antifungal activity of South African indigenous plants against aflatoxigenic Aspergillus species, S. Afr. J. Bot. 115 (2018) 318, https://doi.org/10.1016/J.SAJB.2018.02.153.
[31] D.L.P. Macuvele, G.Z.S. Sithole, K. Cesca, S.L.P. Macuvele, J.V. Matsinhe, Aqueous extracts of Mozambican plants as alternative and environmentally safe acid-base indicators, Environ. Sci. Pollut. Res. 23 (2016) 11639–11644, https://doi.org/10.1007/s11356-016-6284-2.
[32] H.P. Klug, L.E. Alexander, X-ray diffraction procedures: for polycrystalline and amorphous materials, in: H.P. Klug, L.E. Alexander (Eds.), X-Ray Diffr. Proced. Polycryst. Amorph. Mater. 2nd ed., Wiley-VCH, 1974, p. 992 Pp. 992, ISBN 0-471-49369-4, May 1974.
[33] D.F. Swinehart, The Beer-Lambert law, J. Chem. Educ. 39 (1962) 333, https://doi.org/10.1021/ed039p333.
[34] P. Singh, Y.-J. Kim, D. Zhang, D.-C. Yang, Biological synthesis of nanoparticles from plants and microorganisms, Trends Biotechnol. 34 (2016) 588–599, https://doi.org/10.1016/J.TIBTECH.2016.02.006.
[35] R. Septawendar, S. Sutardi, U. Karsono, N. Sofiyaningsih, A. Low-Cost, Facile method on production of nano zirconia and silica from local zircon in a large scale using a sodium carbonate sintering technology, J. Aust. Ceram. Soc. 52 (2016) 92–102.
[36] W. Li, H. Huang, H. Li, W. Zhang, H. Liu, Facile synthesis of pure monoclinic and tetragonal zirconia nanoparticles and their phase effects on the behavior of supported molybdena catalysts for methanol-selective oxidation, Langmuir. 24 (2008) 8358–8366, https://doi.org/10.1021/la800370r.
[37] H.-J. Noh, D.-S. Seo, H. Kim, J.-K. Lee, Synthesis and crystallization of anisotropic shaped ZrO2 nanocrystalline powders by hydrothermal process, Mater. Lett. 57 (2003) 2425–2431, https://doi.org/10.1016/S0167-577X(02)01248-X.
[38] C. Suciu, A.C. Hoffmann, A. Vik, F. Goga, Effect of calcination conditions and precursor proportions on the properties of YSZ nanoparticles obtained by modified sol–gel route, Chem. Eng. J. 138 (2008) 608–615, https://doi.org/10.1016/J.CEJ.2007.09.020.
[39] C.-W. Kuo, Y.-H. Lee, K.-Z. Fung, M.-C. Wang, Effect of Y2O3 addition on the phase transition and growth of YSZ nanocrystallites prepared by a sol–gel process, J. Non. Solids 351 (2005) 304–311, https://doi.org/10.1016/J.JNONCRYSOL.2004.11.002.
[40] M.S. Nouri, A. Kompany, G.H. Khorrami, A.K. Zak, The Effect of calcination temperature on the structure properties of ZrO 2 nanoparticles synthesized by modified sol gel ingelatin media, Iran, J. Crytallogr. Miner. 24 (2017) (2017).
[41] S. Jayakumar, P.V. Ananthapadmanabhan, K. Perumal, T.K. Thiyagarajan, S.C. Mishra, L.T. Su, A.I.Y. Tok, J. Guo, Characterization of nano-crystalline ZrO2 synthesized via reactive plasma processing, Mater. Sci. Eng. B 176 (2011) 894–899, https://doi.org/10.1016/J.MSEB.2011.05.013.
[42] H. Borchert, E.V. Shevchenko, A. Robert, I. Mekis, A. Kornowski, G. Grübel, H. Weller, Determination of nanocrystal sizes: a comparison of TEM, SAXS, and XRD studies of highly monodisperse CoPt3 particles, Langmuir 21 (2005) 1931–1936, https://doi.org/10.1021/la0477183.
[43] F. Davar, A. Majedi, A. Mirzaei, Polyvinyl alcohol thin fi lm reinforced by green synthesized zirconia nanoparticles, Ceram. Int. 44 (2018) 19377–19382, https://doi.org/10.1016/j.ceramint.2018.07.167.
[44] V. Sai Saraswathi, K. Santhakumar, Photocatalytic activity against azo dye and cytotoxicity on MCF-7 cell lines of zirconium oxide nanoparticle mediated using leaves of Lagerstroemia speciosa, J. Photochem. Photobiol. B Biol. 169 (2017) 47–55, https://doi.org/10.1016/J.JPHOTOBIOL.2017.02.023.
[45] M.A. Blesa, A.J.G. Maroto, S.I. Passaggio, N.E. Figliolia, G. Rigotti, Hydrous zirconium dioxide: interfacial properties, the formation of monodisperse spherical particles, and its crystallization at high temperatures, J. Mater. Sci. 20 (1985) 4601–4609, https://doi.org/10.1007/BF00559350.
[46] P.L. Brown, E. Curti, B. Grambow, C. Ekberg, Chemical Thermodynamics of Zirconium, 1st ed, Elsevier Science, France, 2005.
[47] Y. Zhang, L. Wang, J. Tian, H. Li, Y. Luo, X. Sun, Ag@Poly(m-phenylenediamine) core – shell nanoparticles for highly selective, multiplex nucleic acid detection, Langmuir 27 (2011) 2170–2175, https://doi.org/10.1021/la105092f.
[48] S. Jain, M.S. Mehata, Medicinal plant leaf extract and pure flavonoid mediated green synthesis of silver nanoparticles and their enhanced antibacterial property, Sci. Rep. 7 (2017) 1–13, https://doi.org/10.1038/s41598-017-15724-8.
[49] J. Huang, G. Zhan, B. Zheng, D. Sun, F. Lu, Y. Lin, H. Chen, Z. Zheng, Y. Zheng, Q. Li, Biogenic silver nanoparticles by cacumen platycladi extract: synthesis, formation mechanism, and antibacterial activity, Ind. Eng. Chem. Res. 50 (2011) 9095–9106, https://doi.org/10.1021/ie200858y.
[50] O. Weigenand, A.A. Hussein, N. Lall, J.J.M. Meyer, Antibacterial activity of naphthoquinones and triterpenoids from Euclea natalensis root bark, J. Nat. Prod. 67 (2004) 1936–1938, https://doi.org/10.1021/np030465d.
[51] N. Lall, J.J.M. Meyer, Y. Wang, N.B. Bapela, C.E.J. van Rensburg, B. Fourie, S.G. Franzblau, Characterization of intracellular activity of antitubercular constituents the roots of Euclea natalensis, Pharm. Biol. 43 (2005) 353–357, https://doi.org/10.1080/13880200590951829.
[52] L.J. McGaw, N. Lall, T.M. Hlokwe, A.L. Michel, J.J.M. Meyer, J.N. Eloff, Purified Compounds and extracts from *Euclea* species with antimycobacterial activity against *Mycobacterium bovis* and fast-growing mycobacteria, Biol. Pharm. Bull. 31 (2008) 1429–1433, https://doi.org/10.1248/bpb.31.1429.
[53] N. Lall, O. Weiganand, A.A. Hussein, J.J.M. Meyer, Antifungal activity of naphthoquinones and triterpenes isolated from the root bark of Euclea natalensis, S. Afr.

J. Bot. 72 (2006) 579–583, https://doi.org/10.1016/J.SAJB.2006.03.005.
[54] F. van der Kooy, J.J.M. Meyer, N. Lall, Antimycobacterial activity and possible mode of action of newly isolated neodiospyrin and other naphthoquinones from Euclea natalensis, S. Afr. J. Bot. 72 (2006) 349–352, https://doi.org/10.1016/J.SAJB.2005.09.009.
[55] M. Rathod, S. Haldar, S. Basha, Nanocrystalline cellulose for removal of tetracycline hydrochloride from water via biosorption: equilibrium, kinetic and thermodynamic studies, Ecol. Eng. 84 (2015) 240–249, https://doi.org/10.1016/J.ECOLENG.2015.09.031.
[56] H. Wang, Y. Chu, C. Fang, F. Huang, Y. Song, X. Xue, Sorption of tetracycline on biochar derived from rice straw under different temperatures, PLoS One 12 (2017) e0182776, , https://doi.org/10.1371/journal.pone.0182776.
[57] E. Bağda, M. Erşan, E. Bağda, Investigation of adsorptive removal of tetracycline with sponge like, Rosa canina gall extract modified, polyacrylamide cryogels, J. Environ. Chem. Eng. 1 (2013) 1079–1084, https://doi.org/10.1016/J.JECE.2013.08.024.